NOTICE: This is the authors' version of a work that was accepted for publication in International Journal of Geomechanics. Changes resulting from the publishing process, such as peer review, editing, corrections, structural formatting, and other quality control mechanisms may not be reflected in this document. Changes may have been made to this work since it was submitted for publication. A definitive version was subsequently published in International Journal of Geomechanics, 2024. doi: https://doi.org/10.1061/IJGNAI.GMENG-8977

Long-term settlement of dynamically loaded shallow foundations

Patrick Staubach*; Dirk Wegener†; Jan Machaček‡; Torsten Wichtmann§

Abstract: Analytical approaches to determine the long-term settlement of shallow foundations subjected to dynamic cyclic loading with a large number of cycles (millions) are presented. The approaches utilise the high-cycle accumulation (HCA) model to calculate the permanent strain caused by the cyclic loading and are conceptionally similar to conventional settlement analyses. The incorporation of a threshold strain amplitude, below which no accumulation of deformations occurs, in the HCA model is discussed. It is demonstrated that the simple analytical approach, which does not require numerical calculations, gives results very similar to more complex finite element simulations.

Keywords: cyclic loading; dynamics; strain amplitude; high-cycle accumulation model; long-term settlement

*Chair of Geotechnics, Institute of Structural Engineering, Bauhaus-Universität Weimar, Germany/Chair of Soil Mechanics, Foundation Engineering and Environmental Geotechnics, Ruhr Universität Bochum, Germany. Email: patrick.staubach@uni-weimar.de, Corresponding author. ORCID: 0000-0002-1788-4880

†GEPRO Ingenieurgesellschaft mbH, Dresden, Germany

‡Institute of Geotechnics, Technische Universität Darmstadt, Germany/Chair of Soil Mechanics, Foundation Engineering and Environmental Geotechnics, Ruhr-Universität Bochum, Germany. ORCID: 0000-0003-4849-5754

§Chair of Soil Mechanics, Foundation Engineering and Environmental Geotechnics, Ruhr-Universität Bochum, Germany. ORCID: 0000-0002-9250-7014

Introduction

The prediction of permanent displacements caused by cyclic loading is important for the assessment of the stability and serviceability of machine foundations, infrastructure objects or structures subject to wind and water loading. In such cases the frequency of the cyclic loading and the number of load cycles is very high and can be in the range of millions of cycles. The cyclic loading causes wave propagation and thus strains in the soil. Often the magnitude of this strain is so small that the soil responds fully elastically and no permanent deformations accumulate, even if the number of load cycles is in the millions. However, once a certain strain is exceeded, known as threshold strain, plastic deformations occur and can accumulate with increasing number of load cycles.

There are a number of engineering (see e.g. Sawicki and Świdziński, 1989; Lentz and Baladi, 1981; Byrne and McIntyre, 1994; Li and Selig, 1996) and also more sophisticated phenomenological (see e.g. François et al., 2010; Pasten et al., 2014) models that can be used to estimate this accumulation of plastic strains. However, they are often derived for a specific case and can not be applied for arbitrary soils in an arbitrary state. In addition, if accumulation is accounted for in the model, inertia effects are often neglected or vice versa. In general, the more sophisticated approaches require to perform finite element (FE) simulations to calculate settlements, which may render them unhandy for applications in practice.

A practical approach to predict the long-term response of foundations to cyclic loading with high frequencies, which is applicable to any soil in any state, is presented in this work. For this, the high-cycle accumulation (HCA) models are adopted (Niemunis et al., 2005; Wichtmann, 2016), which were developed on the basis of a large number of triaxial tests with a high number of loading cycles (more than 100,000 cycles) on various soils in various states. The necessary incorporation of the threshold strain in the model is discussed and different approaches are presented for its realization. In order to apply the HCA model for simple practical problems, it is recast in 1D form, which allows to perform the calculations analogously to conventional settlement analyses. Therefore, no complex FE simulations are needed.

Shear strain, threshold shear strain and total strain

Shear strain and threshold shear strain

Shear strain is an essential parameter for the assessment of the response of soils to dynamic loading. With increasing shear strain, the stiffness of the soil decreases and the accumulation of permanent strain or pore water pressures increases. According to Dobry and Abdoun, 2015, expressing action in terms of shear strain offers important practical advantages over the cyclic stress ratio (CSR) developed in the 1970s and still used in earthquake engineering today to examine the risk of liquefaction.

Vucetic (1994) and Hsu and Vucetic (2004) showed that at shear strains γ lower than

the volumetric threshold shear strain γ_{tv}, no significant volumetric strains accumulate after a few cycles ($10 \leq N \leq 200$) in drained tests. The same applied to excess pore water pressures built up in undrained tests. These criteria can be used for evaluations of liquefaction triggering as a result of a few cycles, e.g. due to earthquakes. γ_{tv} is very robust according to Dobry and Abdoun (2015). In both clean and silty normally consolidated sands $\gamma_{tv} \approx 0.01$ % (in the range of 0.006 - 0.02 %) is largely independent of the mean effective stress, the exact number of cycles ($10 \leq N \leq 200$), the relative density, the nonplastic fines content and the sand fabric (deposition method) (Dobry and Abdoun, 2015).

Evaluations of cyclic triaxial tests and resonant column tests in (Wichtmann and Triantafyllidis, 2013; Wichtmann et al., 2015a), with much larger numbers of cycles ($N >> 1,000$), show a relatively robust threshold shear strain as well. However, compared to the tests with lower number cycles reported in Vucetic (1994), a slightly lower threshold shear strain $\gamma_{tv} \approx 0.002 - 0.005$ % for clean sand and $\gamma_{tv} \approx 0.004 - 0.012$ % for silty sand (in dependence of the non-cohesive fines content) was observed. The values of γ_{tv} were found to be rather robust in terms of stress, density and grain size distribution. From these results, it is clear that determination of γ_{tv} for a small number of cycles (e.g., several hundred, as reported in Vucetic (1994)) and application to loading with a much larger number of cycles is questionable.

Based on the aforementioned results, it is possible to distinguish between three ranges of strain with different characteristic soil behaviour, as illustrated in Fig. 1. Below the threshold shear strain γ_{tv} no or only very small volumetric strains $\varepsilon_v^{\mathrm{acc}}$ accumulate even with a high number of cycles (Figs. 1a,b). Since the HCA model predicts the soil response to a large number of load cycles, the lower range of the volumetric threshold shear strain γ_{tv} is adopted to calculate the threshold strain amplitude $\varepsilon_{\mathrm{lim}}^{\mathrm{ampl}}$ used in the HCA model, which is discussed in Section *Threshold strain amplitude and its incorporation in the HCA model*.

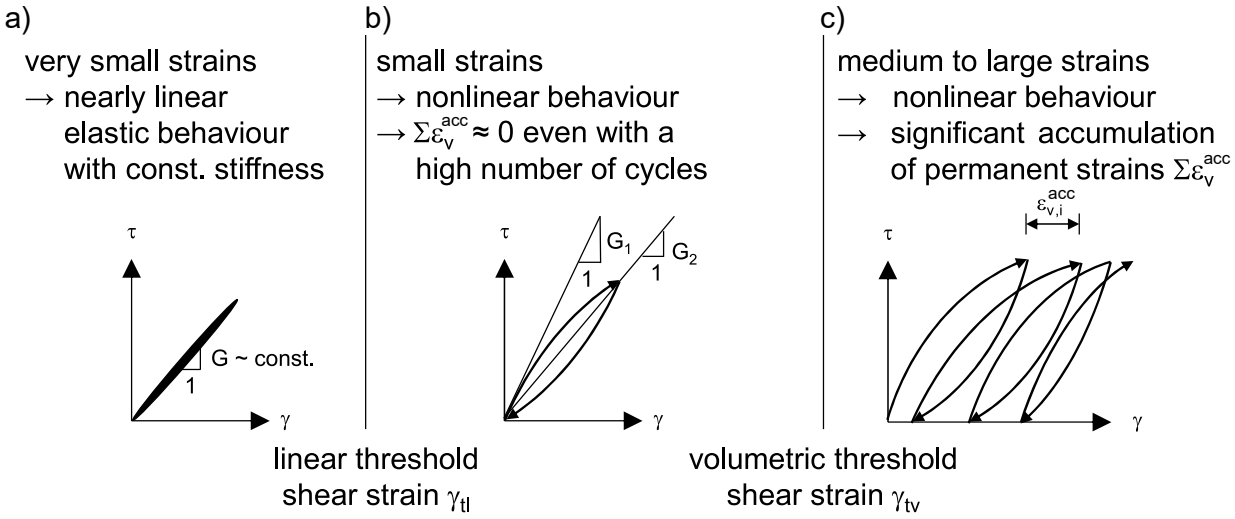

Fig. 1. Typical soil behaviour under cyclic loading in three different strain ranges (plots a-c), with schematic $\gamma_c = \varepsilon_y - \varepsilon_x$ vs. $\tau_c = (\sigma_y - \sigma_x)/2$ diagrams from drained cyclic triaxial tests. $\varepsilon_{v,i}^{\mathrm{acc}}$ is the permanent volumetric strain in cycle i.

Conversion from shear strain to total strain

The HCA model uses the total strain ε and the (total) threshold strain amplitude $\varepsilon_{\text{lim}}^{\text{ampl}}$. Therefore, a conversion of the shear strain γ and the threshold shear strain $\gamma_{tv,0}$ into ε and $\varepsilon_{\text{lim}}^{\text{ampl}}$ is required. The total strain ε is defined in general form in Eq. (1):

$$\varepsilon = ||\boldsymbol{\varepsilon}|| = \sqrt{\varepsilon_{xx}^2 + \varepsilon_{xy}^2 + \varepsilon_{xz}^2 + \varepsilon_{yx}^2 + \varepsilon_{yy}^2 + \varepsilon_{yz}^2 + \varepsilon_{zx}^2 + \varepsilon_{zy}^2 + \varepsilon_{zz}^2} \tag{1}$$

In a simple shear test, the shear strain $\gamma = \gamma_{xy}$ is defined as u_x/Y, see Fig. 2, left. For small strains $\gamma_{xy} = 2\varepsilon_{xy} \approx u_x/Y + u_y/X$ applies, with $u_y/X \approx 0$. The total strain ε is then given by Eq. (1) with $\varepsilon_{xy} = \varepsilon_{yx} = 1/2\gamma_{xy}$:

$$\varepsilon = \sqrt{(\frac{1}{2}\gamma_{xy})^2 + (\frac{1}{2}\gamma_{xy})^2} = \frac{1}{\sqrt{2}} \cdot \gamma_{xy} = \frac{1}{\sqrt{2}} \cdot \gamma \tag{2}$$

In torsional shear tests and in resonant column tests the shear strain γ is also used (Vucetic and Dobry, 1988; Jamiolkowski et al., 1994) and Eq. (2) is valid.

However, in a triaxial test, the shear strain γ_c is defined as $\gamma_c = \varepsilon_y - \varepsilon_x$ with the vertical strain $\varepsilon_y = u_y/Y$ and the horizontal strain $\varepsilon_x = u_x/X$, see Fig. 2, right. The principal strains are $\varepsilon_y \geq \varepsilon_x = \varepsilon_z = -\nu\ \varepsilon_y$ with the Poisson's ratio ν and the other shear strain components are zero. The total strain ε is given by Eq. (3) and the shear strain γ_c is defined in Eq. (4). It should be noted that γ_c is convert to γ with the factor $\sqrt{3}/2$, because of the conversion of the equivalent invariant shear strain, see explanations in Wegener and Herle (2012) and Section 2.4.3 in Wegener (2013). Based on Eq. (4), this results in Eq. (5).

$$\varepsilon = \sqrt{\varepsilon_y^2 + 2(-\nu \cdot \varepsilon_y)^2} = \sqrt{1 + 2\ \nu^2} \cdot \varepsilon_y \tag{3}$$

$$\gamma_c = \varepsilon_y - \varepsilon_x = (1 + \nu) \cdot \varepsilon_y \tag{4}$$

$$\gamma = 2/\sqrt{3} \cdot \gamma_c = 2/\sqrt{3}\ \ (1 + \nu) \cdot \varepsilon_y \tag{5}$$

From Eqs. (3) and (5) a relation between ε and γ for triaxial tests results, given by Eq. (6):

$$\varepsilon = \frac{\sqrt{3}}{2} \cdot \frac{\sqrt{1 + 2\ \nu^2}}{1 + \nu} \cdot \gamma \tag{6}$$

The relation between ε and γ for triaxial tests depends on ν. It results for

- $\nu = 0.30$ (drained): $\varepsilon \approx 0.724 \cdot \gamma \approx 1.023/\sqrt{2} \cdot \gamma$,
- $\nu = 0.40$ (drained): $\varepsilon \approx 0.711 \cdot \gamma \approx 1.005/\sqrt{2} \cdot \gamma$ and
- $\nu = 0.50$ (undrained): $\varepsilon = 1/\sqrt{2} \cdot \gamma$ as in Eq. (2) for simple shear tests.

From the previous considerations it can be concluded that Eq. (2) can generally be used as an approximation, i.e. $\varepsilon \approx 1/\sqrt{2} \cdot \gamma$.

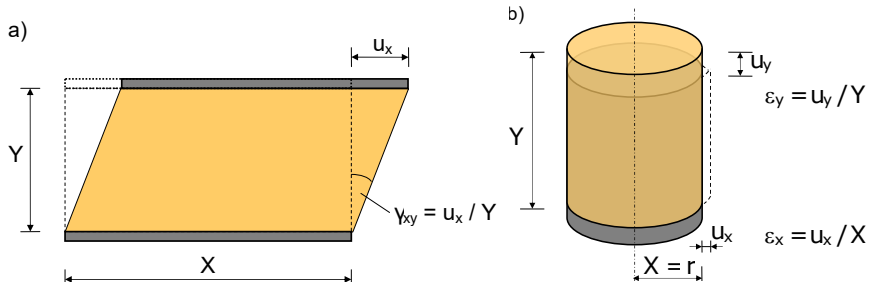

Fig. 2. a) Shear strain $\gamma = \gamma_{xy}$ in a simple shear test; b) Principal strains ε_x and ε_y with shear strain $\gamma_c = \varepsilon_y - \varepsilon_x$ in a triaxial test

The HCA model, its 1D formulation and threshold strain amplitude

HCA model

The simulations with the HCA model are conceptually divided into a low-cycle (sometimes denoted as "implicit") and a high-cycle (sometimes denoted as "explicit") mode. In the low-cycle mode a conventional calculation is performed using a common constitutive model (a simple elastic model is used in the present study). The strain amplitude $\varepsilon^{\mathrm{ampl}}$, which can be interpreted as a state variable of the HCA model, is determined in each element based on the strain path recorded during an individual load cycle. As depicted in Fig. 3, this can either be the second cycle or a so-called update cycle. Based on the recorded six-dimensional strain path (six independent components of the strain tensor for 3D cases), the strain amplitude is defined as the Euclidean norm of six spans which are obtained by consecutive projection (degeneration) on (hyper-) planes (for details see Niemunis et al., 2005).

In the high-cycle mode the accumulation trend is predicted by the HCA model for a given number of loading cycles, using the evaluated strain amplitude as input. This calculation strategy is illustrated in the scheme of Figure 3. During the high-cycle phases the strain amplitude is assumed constant. The field of the strain amplitude can be updated in an update cycle, which is simulated in the low-cycle mode again. Alternatively, the adaptive strain amplitude proposed in Staubach et al. (2022a) can be used, which allows for a continuous update of $\varepsilon^{\mathrm{ampl}}$. During the high-cycle phase only the changes of the average values of stress, strain and other state variables for a given increment ΔN of the number of cycles are calculated.

In the high-cycle mode, stress and strain rates are interrelated by:

$$\dot{\boldsymbol{\sigma}} = \mathsf{E} : (\dot{\boldsymbol{\varepsilon}} - \dot{\boldsymbol{\varepsilon}}^{\mathrm{acc}} - \dot{\boldsymbol{\varepsilon}}^{\mathrm{pl}}) \tag{7}$$

Therein, the stress rate $\dot{\boldsymbol{\sigma}}$ of the effective Cauchy stress $\boldsymbol{\sigma}$ (compression positive), the strain rate $\dot{\boldsymbol{\varepsilon}}$ (compression positive), the accumulation rate $\dot{\boldsymbol{\varepsilon}}^{\mathrm{acc}}$, a plastic strain rate $\dot{\boldsymbol{\varepsilon}}^{\mathrm{pl}}$ (necessary only for stress paths touching the yield surface) and the barotropic elastic stiffness E are used. In the context of HCA models the dot over a symbol denotes the derivative with

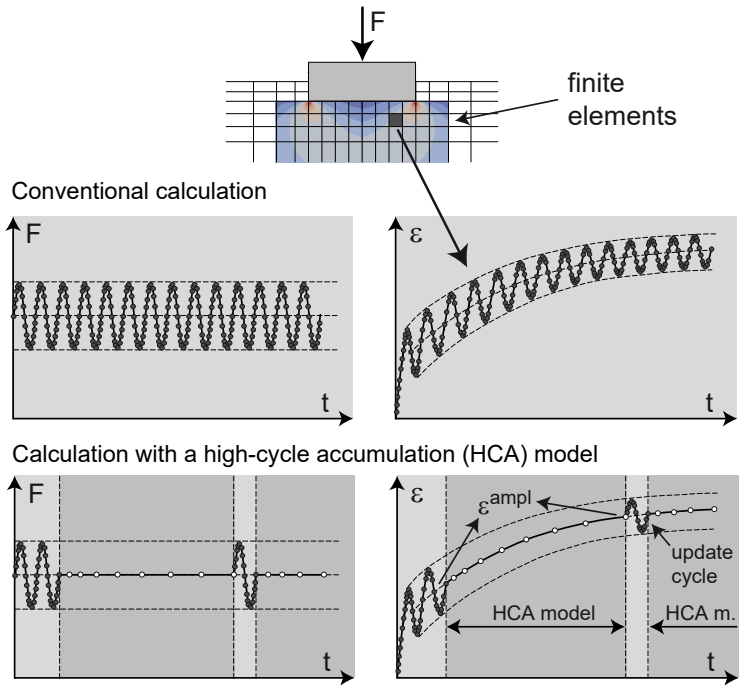

Fig. 3. Calculation strategy for simulations with the HCA model. The strain amplitude $\varepsilon^{\mathrm{ampl}}$ is determined from the second load cycle calculated with a conventional constitutive model. Only the strain accumulation trend is predicted in the high-cycle phase.

respect to the number of cycles N (instead of time t), i.e. $\dot{\square} = \partial \square / \partial N$. Depending on the boundary conditions, Eq. (7) predicts a change of stress ($\dot{\boldsymbol{\sigma}} \neq \mathbf{0}$) and / or an accumulation of strain ($\dot{\boldsymbol{\varepsilon}} \neq \mathbf{0}$).

For $\dot{\boldsymbol{\varepsilon}}^{\mathrm{acc}}$ in Eq. (7) the following multiplicative approach is used:

$$\dot{\boldsymbol{\varepsilon}}^{\mathrm{acc}} = \dot{\varepsilon}^{\mathrm{acc}}\ \mathbf{m} \tag{8}$$

with the *direction* of strain accumulation (flow rule) $\mathbf{m} = \dot{\boldsymbol{\varepsilon}}^{\mathrm{acc}} / \|\dot{\boldsymbol{\varepsilon}}^{\mathrm{acc}}\| = (\dot{\boldsymbol{\varepsilon}}^{\mathrm{acc}})^{\rightarrow}$ (unit tensor) and the *intensity* of strain accumulation $\dot{\varepsilon}^{\mathrm{acc}} = \|\dot{\boldsymbol{\varepsilon}}^{\mathrm{acc}}\|$. The flow rule of the Modified Cam Clay (MCC) model is applied for $\mathbf{m}$.

The intensity of strain accumulation $\dot{\varepsilon}^{\mathrm{acc}}$ in Eq. (8) is calculated as a product of six functions (Niemunis et al., 2005):

$$\dot{\varepsilon}^{\mathrm{acc}} = f_{\mathrm{ampl}}\ \dot{f}_N\ f_e\ f_p\ f_Y\ f_\pi \tag{9}$$

each considering a single influencing parameter (see Table 1), i.e. the strain amplitude $\varepsilon^{\mathrm{ampl}}$ (function f_{ampl}), the cyclic preloading ($\dot{f}_N$, using the preloading variable g^A which weights the number N of applied cycles with the strain amplitude $\varepsilon^{\mathrm{ampl}}$ of these cycles), void ratio e (f_e), average mean stress p^{av} (f_p), normalized average stress ratio $\bar{Y}^{\mathrm{av}}$ (f_Y, $\bar{Y}^{\mathrm{av}} = 0$ at isotropic stresses, $\bar{Y}^{\mathrm{av}} = 1$ at critical stress ratio) and the effect of polarization changes ($f_\pi = 1$ for a constant direction of cyclic loading). Note that the term $C_e - e^{\mathrm{av}}$ in function f_e is not allowed to take positive values, i.e. it is zero for $C_e - e^{\mathrm{av}} \geq 0$. The function f_e tends to zero as the void ratio tends to the value of parameter C_e, i.e. reaching a so-called

Function	Material constants
$f_{\text{ampl}} = \min\left\{\left(\frac{\varepsilon^{\text{ampl}}}{10^{-4}}\right)^{C_{\text{ampl}}}; 10^{C_{\text{ampl}}}\right\}$	C_{ampl}
$\dot{f}_N = \dot{f}_N^A + \dot{f}_N^B$ $\dot{f}_N^A = C_{N1}C_{N2}\exp\left[-\frac{g^A}{C_{N1}f_{\text{ampl}}}\right]$ $\dot{f}_N^B = C_{N1}C_{N3}$	C_{N1} C_{N2} C_{N3}
$f_e = \frac{(C_e - e)^2}{1+e}\,\frac{1+e_{\max}}{(C_e - e_{\max})^2}$	C_e
$f_p = \exp\left[-C_p\left(\frac{p^{\text{av}}}{100\ \text{kPa}} - 1\right)\right]$	C_p
$f_Y = \exp\left(C_Y\ \bar{Y}^{\text{av}}\right)$	C_Y

Table 1. Summary of the functions and material constants of the HCA model. Note that $f_\pi = 1$ holds for constant polarization, which is why its function is not given here. It is discussed in Wichtmann, 2005.

terminal void ratio (Narsilio and Santamarina, 2008). This is also the reason for $f_e = 0$ if $C_e - e^{\text{av}} \geq 0$.

The equations of the HCA model are based on comprehensive experimental parametric studies documented in Wichtmann (2005) and Wichtmann et al. (2005). For a more detailed discussion of the HCA model the interested reader is referred to Niemunis et al. (2005) and Wichtmann (2016). The parameters of the HCA model can be determined from experiments (Wichtmann et al., 2010; Wichtmann et al., 2015b) or estimated based on granulometry or simple index quantities (Wichtmann et al., 2009; Wichtmann et al., 2015b). In a very recent study (Birrell et al., 2022), probabilistic characterisation of the HCA model parameters and Bayesian parameter estimation were undertaken.

Simplified HCA model for 1D analyses

In order to allow for an analytical calculation of the strain accumulation below a foundation analogously to a conventional settlement analysis, a simplified HCA model for 1D analyses is derived in this section. The following assumptions are made:

- $\dot{\boldsymbol{\sigma}} = \mathbf{0}$: The accumulation of strain due to stress cycles is not prevented by boundary conditions, which results in constant average stress. For example, this is the case in a drained cyclic triaxial test, where an unrestrained accumulation of strain can occur. It is also a justified assumption for the settlement analysis of foundations since the soil is rather free in accumulating strains. However, the relaxation of stress due to densification is not accounted for. The assumption of $\dot{\boldsymbol{\sigma}} = \mathbf{0}$ has also relevant implications for the application of the simplified version of the HCA model to the simulation of a dynamic boundary value problem. For this it has to be assumed that the accumulation of permanent strains does not lead to a change in the mean

acceleration. In that case it is sufficient to calculate the strain amplitude in a dynamic analysis and perform the high-cycle calculation neglecting the inertial forces, as their effect is included in the strain amplitude. The larger the stress rate, the less justified is the assumption that the average acceleration is constant, since the momentum balance then requires changes in acceleration to ensure equilibrium.

- $\dot{\boldsymbol{\varepsilon}}^{\mathrm{pl}} = \mathbf{0}$: The stresses never reach the failure surface. Since $\dot{\boldsymbol{\sigma}} = \mathbf{0}$ holds, and the initial stress is within the Matsuoka-Nakai surface, this assumption is automatically satisfied.

Because the direction of strain accumulation $\mathbf{m}$ is not required for 1D conditions, the following simple form of Eq. (7) is obtained adopting the assumptions listed above:

$$\dot{\varepsilon} = \dot{\varepsilon}^{\mathrm{acc}} = f_{\mathrm{ampl}}\ \dot{f}_N\ f_e\ f_p\ f_Y \tag{10}$$

Threshold strain amplitude and its incorporation in the HCA model

In order to incorporate the threshold strain amplitude described in Section *Shear strain and threshold shear strain* into the HCA model, three different approaches are schematically shown in Fig. 4. Up to now, the function f_{ampl} is (usually) a non-linear function in $\varepsilon^{\mathrm{ampl}}$ not considering $\varepsilon_{\mathrm{lim}}^{\mathrm{ampl}}$ (or only a very low value of 10^{-7}), which is indicated by the dashed line in Fig. 4. To incorporate $\varepsilon_{\mathrm{lim}}^{\mathrm{ampl}}$, three approaches are investigated:

1) Setting the function f_{ampl} to zero for $\varepsilon^{\mathrm{ampl}} \leq \varepsilon_{\mathrm{lim}}^{\mathrm{ampl}}$ but using the regular function for $\varepsilon^{\mathrm{ampl}} > \varepsilon_{\mathrm{lim}}^{\mathrm{ampl}}$, i.e.

$$f_{\mathrm{ampl}} = \begin{cases} 0 & \text{for } \varepsilon^{\mathrm{ampl}} \leq \varepsilon_{\mathrm{lim}}^{\mathrm{ampl}} \\ \left(\dfrac{\varepsilon^{\mathrm{ampl}}}{10^{-4}}\right)^{C_{\mathrm{ampl}}} & \text{for } \varepsilon^{\mathrm{ampl}} > \varepsilon_{\mathrm{lim}}^{\mathrm{ampl}} \end{cases} \tag{11}$$

2) Considering $\varepsilon_{\mathrm{lim}}^{\mathrm{ampl}}$ directly in the function of f_{ampl}, i.e.

$$f_{\mathrm{ampl}} = \begin{cases} 0 & \text{for } \varepsilon^{\mathrm{ampl}} \leq \varepsilon_{\mathrm{lim}}^{\mathrm{ampl}} \\ \left(\dfrac{\varepsilon^{\mathrm{ampl}} - \varepsilon_{\mathrm{lim}}^{\mathrm{ampl}}}{10^{-4}}\right)^{C_{\mathrm{ampl}}} & \text{for } \varepsilon^{\mathrm{ampl}} > \varepsilon_{\mathrm{lim}}^{\mathrm{ampl}} \end{cases} \tag{12}$$

Without modifying C_{ampl}, this will result in a shift of the value of f_{ampl} with respect to $\varepsilon^{\mathrm{ampl}}$ compared to the first approach and therefore a lower accumulation for all values of $\varepsilon^{\mathrm{ampl}}$.

3) In approach No. 3, Eq. (12) is adopted as well but the parameter C_{ampl} is calibrated anew such that with increasing $\varepsilon^{\mathrm{ampl}}$ the original function of f_{ampl} is obtained. This procedure is equivalent to considering Eq. (12) already when calibrating the parameters based on drained cyclic triaxial tests. Since the different functions and parameters

of the HCA model only work as a set, all parameters potentially change when C_{ampl} is adjusted.

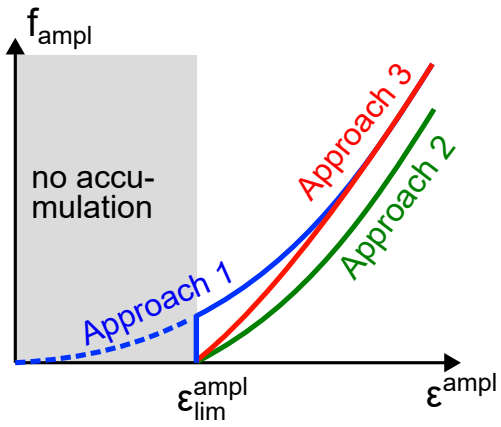

Fig. 4. Different approaches to incorporate a threshold strain amplitude into the function f_{ampl}

Considering that approach No. 3 is rather cumbersome, since none of the existing HCA parameter sets for various soils can directly be used but a re-calibration of parameters is required, approaches Nos. 1 and 2 offer a far more convenient solution. The practical

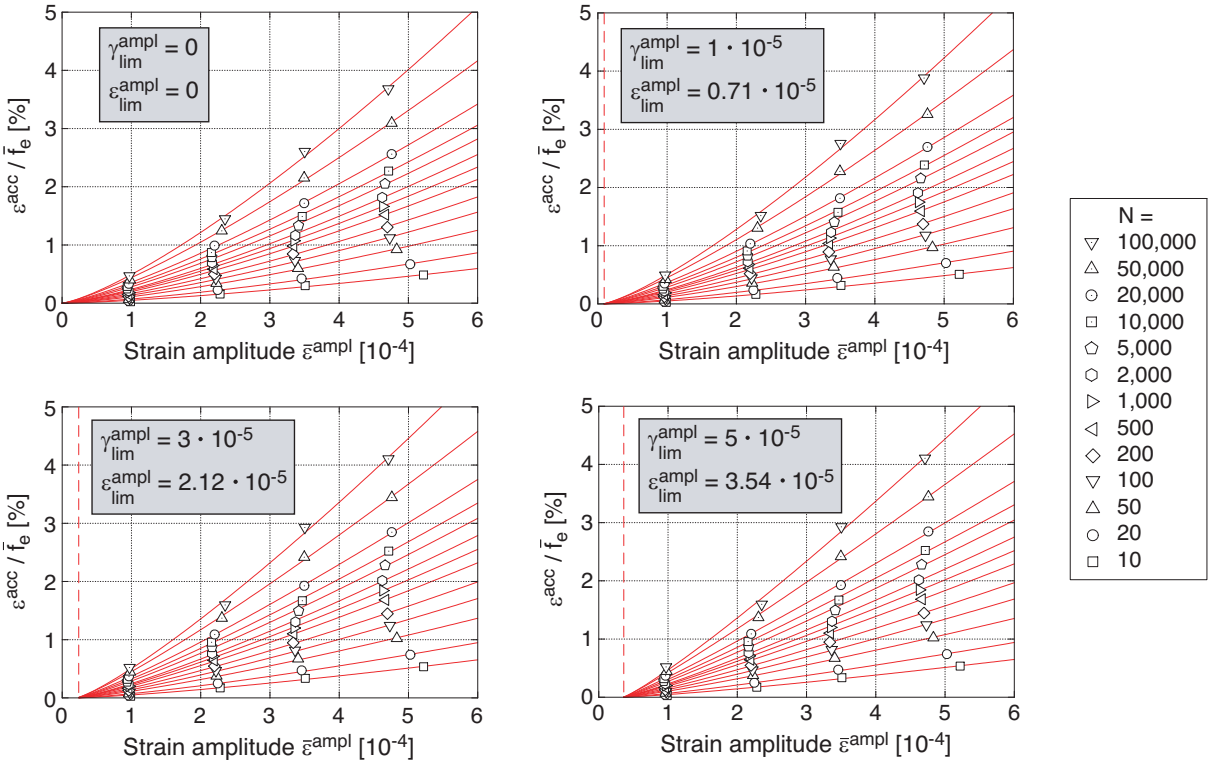

Fig. 5. Calibration of the parameter C_{ampl} based on four drained cyclic triaxial tests with different strain amplitudes considering different values of $\gamma_{\mathrm{lim}}^{\mathrm{ampl}}$ or $\varepsilon_{\mathrm{lim}}^{\mathrm{ampl}}$, respectively

application of approach No. 3 is discussed in the following. Table 2 gives the HCA parameters of Karlsruhe fine sand (KFS) ($D_{50} = 0.14$ mm, $C_U = 1.5$), for which the calibration procedure is described in detail in Wichtmann (2016). This calibration has been performed

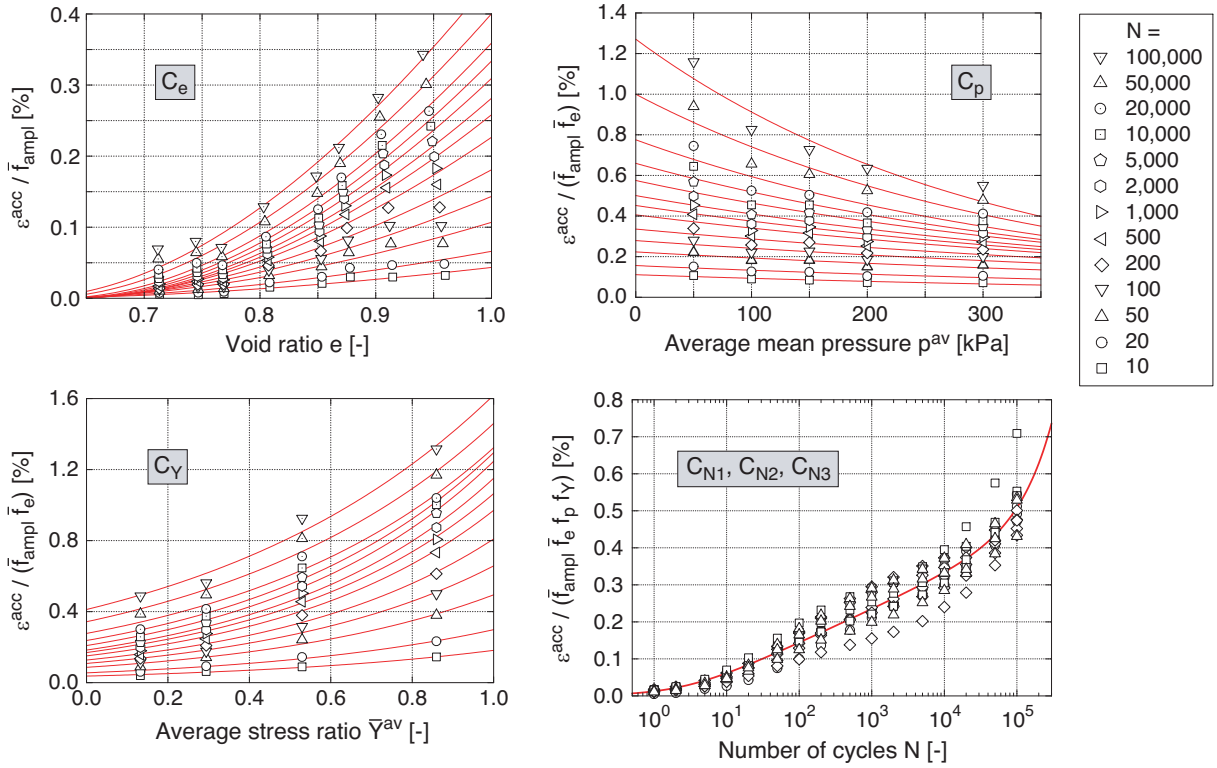

Fig. 6. Calibration of the parameters C_e, C_p and C_Y based on drained cyclic triaxial tests with different void ratio, mean effective stress and stress ratio considering $\gamma_{\text{lim}}^{\text{ampl}} = 3 \cdot 10^{-5}$. The parameters C_{N1}, C_{N2} and C_{N3} are determined using the results of all triaxial tests.

without considering $\varepsilon_{\text{lim}}^{\text{ampl}}$. In Fig. 5 the calibration of C_{ampl} is shown for different values of $\varepsilon_{\text{lim}}^{\text{ampl}}$ considered in Eq. (12). Typical values of $\varepsilon_{\text{lim}}^{\text{ampl}}$ found in experimental studies are considered, see Section *Shear strain and threshold shear strain*. Four drained cyclic triaxial tests with varying deviatoric stress amplitude, but identical average stress ratio, identical average mean effective stress and similar initial void ratio are used for the calibration of C_{ampl}. For each test the accumulated strain ε^{acc} divided by the void ratio function f_e of the HCA model is given for a different number of cycles N. By dividing ε^{acc} by f_e, it is considered that the initial void ratio differs slightly from test to test and is reduced with increasing number of cycles, the latter being more pronounced in case of higher strain amplitudes. By the division of f_e the influence of the void ratio on ε^{acc} is eliminated. The curves approximating the experimental data for a certain number of cycles have been obtained from a curve-fitting using the function f_{ampl} resulting in C_{ampl}. This is done considering three different values of $\gamma_{\text{lim}}^{\text{ampl}}$: $0,1 \cdot 10^{-5}$, $3 \cdot 10^{-5}$ and $5 \cdot 10^{-5}$. The corresponding values of $\varepsilon_{\text{lim}}^{\text{ampl}}$ are given by the dashed vertical line in each plot. Table 2 gives the values of C_{ampl} for each value of $\gamma_{\text{lim}}^{\text{ampl}}$, with the C_{ampl} values representing average values determined from the individual values obtained for the different numbers of cycles. The results of the calibration of the other parameters of the HCA model are given for one specific value of $\gamma_{\text{lim}}^{\text{ampl}} = 3 \cdot 10^{-5}$ in Fig. 6. The optimal parameters for all considered values of $\gamma_{\text{lim}}^{\text{ampl}}$ are summarised in Table 2.

$\gamma_{\text{lim}}^{\text{ampl}}$	$\varepsilon_{\text{lim}}^{\text{ampl}}$	C_{ampl}	C_e	C_p	C_Y	C_{N1} $[10^{-4}]$	C_{N2}	C_{N3} $[10^{-5}]$
0	0	1.32	0.60	0.24	1.74	3.03	0.37	2.36
$1 \cdot 10^{-5}$	$0.71 \cdot 10^{-5}$	1.29	0.61	0.23	1.72	3.31	0.38	2.30
$3 \cdot 10^{-5}$	$2.12 \cdot 10^{-5}$	1.22	0.62	0.21	1.70	3.95	0.37	2.33
$5 \cdot 10^{-5}$	$3.54 \cdot 10^{-5}$	1.15	0.62	0.19	1.68	4.50	0.37	2.33

Table 2. Parameters of the HCA model for Karlsruhe fine sand (KFS) for different values of $\varepsilon_{\text{lim}}^{\text{ampl}}$

Long-term settlement analysis of a dynamically loaded shallow foundation

Task definition

According to an example of the "Empfehlungen des Arbeitskreises Baugrunddynamik" ("Recommendations of the working group Soil Dynamics") (DGGT, 2018), permanent displacements of a machine foundation shall be determined. The geometry and mass of the machine foundation are given in Fig. 7.

The data of the machine and the foundation are as follows

- Cyclic vertical load amplitude $P_0 = 4.0$ kN,
- Frequency of the cyclic load $f = 16.0$ Hz,
- Angular frequency of the cyclic load $\Omega = 2 \cdot \pi \cdot f = 100.5$ Hz,
- Mass of the foundation $m_F = \gamma_F \cdot 2a \cdot 2b \cdot h = 25\ \text{kN/m}^3 \cdot (2.60\ \text{m})^2 \cdot 1.00\ \text{m} = 16.9$ t,
- Total mass of the machine $m_M = 15.0$ t.

Analytical approach

The analytical calculation is performed in analogy to a conventional settlement analysis. The subsoil is divided into several layers in order to take into account the non-linear distribution of the additional stress due to the foundation. The following steps are performed:

1) The cyclic displacement amplitude U_z (in steady state) and the velocity amplitude $V_z = \Omega \cdot U_z$ of the foundation are calculated using the angular frequency of the cyclic load Ω, see Section *Cyclic displacement and velocity amplitude of the foundation*.

2) The velocity in the middle of a layer in the depth z_i is estimated, based on the wave propagation in elastic half spaces (see e.g. Achenbach, 1980; Haupt, 1986), by:

$$V_{z,i} = \begin{cases} V_z & \text{for} \quad z_i \le r_0 \\ V_z \left(\dfrac{z_i}{r_0} \right)^{-n} \cdot e^{-\alpha(z_i - r_0)} & \text{for} \quad z_i > r_0 \end{cases} \tag{13}$$

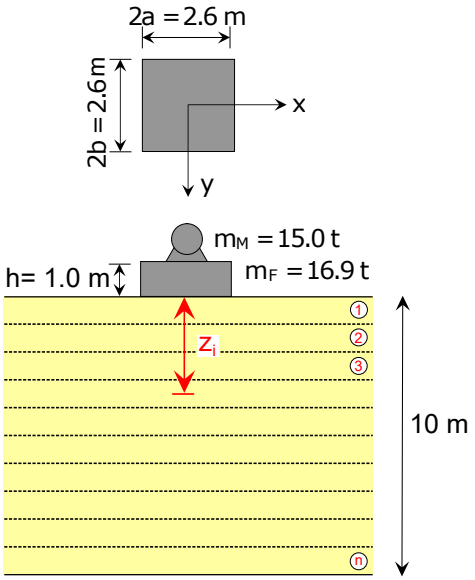

Fig. 7. Geometry and mass of the machine foundation. Division of the subsoil into layers i with distance z_i between bottom of foundation and centre of each layer

with the approximate coefficient for geometrical damping $n = 1$ for the wave propagation for nearly a point load on a half space. n is 1.0 for pure Rayleigh waves and 0.50 for shear and compression waves. The coefficient for material damping is defined as $\alpha \approx 2\pi \cdot D/\lambda$ with the damping ratio $D = 0.02$ and the wavelength $\lambda = c_s/f = 211$ m/s/16 Hz $= 13.2$ m. $n = 1$ is adopted for the analyses presented later.

3) The shear strain can roughly be estimated using the shear wave velocity c_s for dynamic problems for $f > 10$ Hz or $f > 0.4f_0$ with the frequency-independent, undamped natural frequency $f_0 = 1/(2\pi)\sqrt{K_{z,0}/m}$ where in the example the total mass is $m = 31.9$ t and $K_{z,0} = 784,000$ kN/m according to Eq. (17). The wave propagation can be attributed to an approximately one-dimensional problem and, according to the derivations in Achenbach (1980), the shear strain is approximated by:

$$\gamma_i \approx \frac{V_{z,i}}{c_s} \tag{14}$$

For more accurate calculations and low-frequency excitations the shear strains should be calculated by FE analyses, according to Section *Semi-analytical approach*.

4) The strain amplitude entering the HCA model is calculated by $\varepsilon_i^{\text{ampl}} = \gamma_i/\sqrt{2}$, according to Section *Conversion from shear strain to total strain*.

5) Calculation of the initial vertical and horizontal stress σ_v and σ_h due to gravity in each layer considering the additional static load of the foundation and the machine using analytical solutions for elastic half-spaces. The stress is determined in the characteristic point.

6) Calculation of the average mean stress $p^{\mathrm{av}} = (\sigma_v + 2 \cdot \sigma_h)/3$, the deviatoric stress $q^{\mathrm{av}} = \sigma_v - \sigma_h$ and the stress ratio $\eta^{\mathrm{av}} = q^{\mathrm{av}}/p^{\mathrm{av}}$. The lateral stress coefficient $K = \sigma_h/\sigma_v = 0.50$ yields $p^{\mathrm{av}} = 2/3 \cdot \sigma_v$, $q^{\mathrm{av}} = 1/2 \cdot \sigma_v$ and $\eta^{\mathrm{av}} = 0.75$.

7) The accumulated strain at a number of cycles N following Eq. (10) is obtained by:

$$\varepsilon_i^{\mathrm{acc}}(N) = f_{\mathrm{ampl},i}\ f_{e,i}(N)\ f_{p,i}\ f_{Y,i}\ f_{N,i}(N) \tag{15}$$

The change in void ratio entering Eq. (15) by $f_{e,i}(N)$ is taken into account using the mass balance of the solid phase:

$$e_i^{\mathrm{av}}(N) = e_i^{\mathrm{av}}(N - \Delta N) + \varepsilon_i^{\mathrm{acc}}(N) \cdot [1 + e_i^{\mathrm{av}}(N - \Delta N)] \tag{16}$$

8) The settlement is obtained by integration of the accumulated strain in each layer

Cyclic displacement and velocity amplitude of the foundation

The cyclic displacement amplitude U_z of the foundation depends on the frequency-independent spring stiffness $K_{z,0}$ of a substitute circular foundation with a radius of $r_0 = \sqrt{4/\pi} \cdot a = \sqrt{4/\pi} \cdot 1.30\ \mathrm{m} = 1.47\ \mathrm{m}$, which is given as follows (Richart et al., 1970):

$$K_{z,0} = \frac{4 \cdot G \cdot r_0}{1 - \nu} = \frac{4 \cdot 80\ \mathrm{MPa} \cdot 1.47\ \mathrm{m}}{1 - 0.40} = 784,000\ \mathrm{kN/m} \tag{17}$$

The dimensionless frequency a_0 results from the excitation angular velocity $\Omega = 100.5$ Hz in Eq. (18).

$$a_0 = \frac{a \cdot \Omega}{c_s} = \frac{1.30\ \mathrm{m} \cdot 100.5\ \mathrm{Hz}}{211\ \mathrm{m/s}} = 0.62 \tag{18}$$

For a_0 and $b/a = 1.0$ the spring stiffness coefficient is $k_{zz,0\to\Omega} = 0.94$ and the damper coefficient $d_{zz,0\to\Omega} = 0.92$ according to Fig. 8 (Fig. E3-9 from DGGT, 2018). The frequency-dependent spring stiffness $K_{z,\Omega}$ is calculated by Eq. (19) and the frequency-dependent damper $C_{z,\Omega}$ by Eq. (20).

$$K_{z,\Omega} = K_{z,0} \cdot k_{zz,0\to\Omega} = 784,000\ \mathrm{kN/m} \cdot 0.94 = 737,000\ \mathrm{kN/m} \tag{19}$$

$$C_{z,\Omega} = K_{z,0} \cdot \frac{a_0}{\Omega} \cdot d_{zz,0\to\Omega} = 784,000\ \mathrm{kN/m} \cdot \frac{0.62}{100.5\ \mathrm{Hz}} \cdot 0.92 = 4,450\ \mathrm{kN/(m/s)} \tag{20}$$

The cyclic displacement amplitude U_z of the foundation is obtained from Eq. (21) as the quotient of the excitation force amplitude and the absolute value of the complex spring

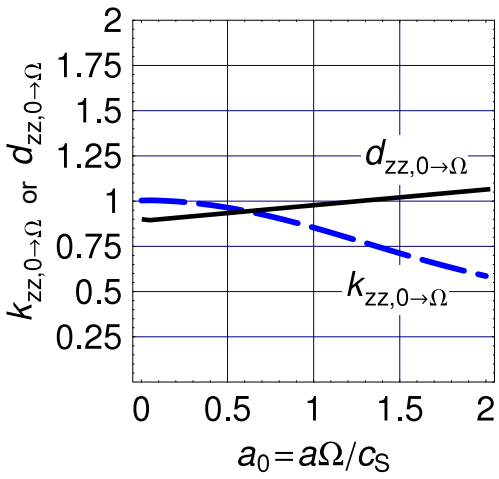

Fig. 8. Spring stiffness coefficient $k_{zz,0\to\Omega}$ and damper coefficient $d_{sz,0\to\Omega}$ modified from DGGT, 2018, Fig. E3-9 based on (Pais and Kausel, 1988; Gazetas, 1991).

stiffness (DGGT, 2018):

$$U_z = |\hat{U}_z| = \frac{P_z}{\sqrt{[K_{z,\Omega} - m \cdot \Omega^2]^2 + [\Omega \cdot C_{z,\Omega}]^2}} \tag{21}$$
$$= \frac{4.0 \text{ kN}}{\sqrt{[737,000 \text{ kN/m} - 31.9 \text{ t} \cdot (100.5 \text{ Hz})^2]^2 + [100.5 \text{ Hz} \cdot 4,450 \text{ kN/(m/s)}]^2}}$$
$$= 6.56 \cdot 10^{-6} \text{ m}$$

The cyclic velocity amplitude V_z bis given by Eq. (22):

$$V_z = \Omega \cdot U_z = 100.5 \text{ Hz} \cdot 6.56 \cdot 10^{-6} \text{ m} = 0.66 \text{ mm/s} \tag{22}$$

Semi-analytical approach

The analytical calculation requires a number of assumptions, in particular for the calculation of the strain amplitude as given in Eq. (14). Therefore, as an alternative, the calculation of the strain amplitude $\varepsilon_i^{\text{ampl}}$ can be carried out in the framework of a FE simulation. A simple elastic dynamic calculation is sufficient to calculate the strain amplitude. The FE-model is described in the next section. The strain amplitude can be determined in the middle of a layer i in the characteristic point, i.e. in the distance of $0.845 \cdot r_0 = 1.24$ m, as the Frobenius norm of the distance of minimum and maximum strain. Only if the loading is not sinusoidal, the projection procedure described in Section *The HCA model, its 1D formulation and threshold strain amplitude* is required. The steps 1) to 5) in Section *Analytical approach* are not necessary in the semi-analytical approach. The strain amplitude obtained from the FE analysis is then inserted in Eq. (15) to calculate the accumulated strain and the settlement of the foundation.

Finite element approach

The specifications of the model, the material parameters and the meshing are shown in Fig. 9. The FE program `numgeo` (Machaček & Staubach, see Machaček (2020), Machaček et al. (2021), Staubach et al. (2022c), and Staubach et al. (2023a) and `www.numgeo.de`) is used. The quadratic foundation in Fig. 7 is replaced by a circular foundation with identical area having a radius of $r_0 = 1.47$ m.

Linearly interpolated axisymmetric elements with four nodes and one integration point are used. The hourglass stiffness is set to 100 kPa. The stress below the foundation results from the dead weights of the machine and foundation, which amounts to $\sigma^{\text{static}} = 47.1$ kPa. An additional dynamic stress σ^{dyn}, with a sinusoidal time-history and a frequency of 16 Hz, is considered, the amplitude of which is varied. The soil is modelled linearly elastic with the parameters given in Table 3 during the low-cycle phase of the calculations.

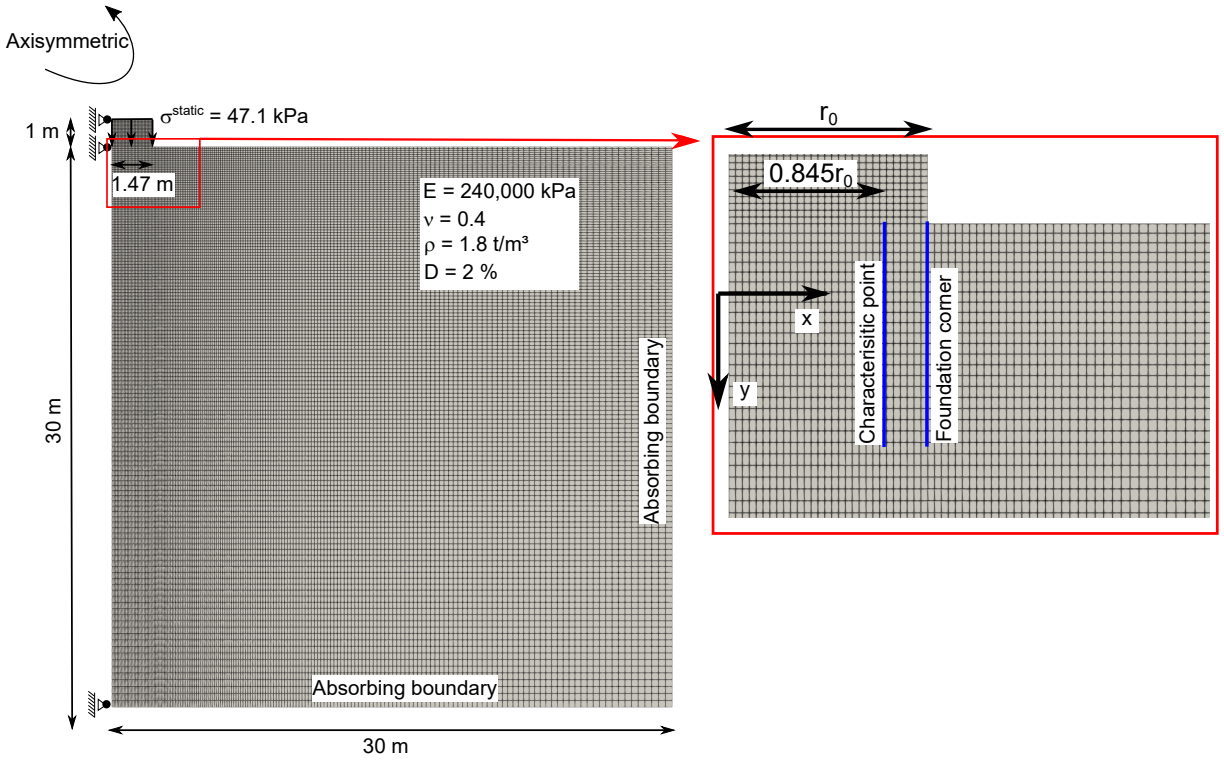

Fig. 9. Model specifications and mesh

Density	Shear modulus	Damping ratio	Poisson's ratio	Shear wave vel.	Stress ratio
ρ [g/cm^3]	G [kPa]	D [-]	ν [-]	c_s [m/s]	$K = \sigma_h \,/\, \sigma_v$ [-]
1.80	80,000	0.02	0.40	211	0.50

Table 3. Soil parameters adopted for the example

The time integration is performed using the Backward Euler (BWE) scheme, which results in a rather strong numerical damping. In preliminary simulations the results were compared to the Hilber-Hughes-Taylor (HHT) scheme, which allows to adjust the numerical damping and minimize its effect. Using parameters resulting in minimum numerical

damping, the displacement amplitude of the foundation during application of σ^{dyn} was approximately 10 % higher with the HHT scheme compared to BWE. However, since the displacement amplitude of the foundation obtained from the FE simulation is used as an input to the analytical calculation, this does not influence the outcome of the comparison of the two approaches. Besides numerical damping, Rayleigh damping is considered with the parameters $\alpha = 2.681$ and $\beta = 0.0001326$ resulting in a damping ratio of approximately $D = 2$ % at a frequency of 16 Hz, see Table 3.

The foundation and soil do not share nodes. A mortar contact discretisation scheme is employed to enforce the non-penetration condition (Staubach et al., 2022c). No friction between soil and foundation is considered.

Lysmer/Kuhlemeyer dampers with the parameters $C_1 = C_2 = 1.0$ are placed at the bottom and right edges of the FE-model to avoid any reflections. More details on the kind of absorbing boundaries implemented in `numgeo` can be found in Machaček (2020) and Schmüdderich et al. (2022). The dimensions of the soil area are 30 × 30 m. This is more than twice the wavelength $\lambda = c_s/f = 211$ m/s/16 Hz = 13.2 m.

The following steps are performed:

1) Simulation of 9 cycles (9/16 Hz = 0.5625 s) using time increments of $\Delta t = 5 \cdot 10^{-4}$ s

2) Recording of the strain path in the 10th cycle (between 0.5625 s and 0.625 s)

3) After the recording cycle, a "resting step" with a duration of 0.3 s is introduced to take into account the decay of the wave propagation. Deactivation of the cyclic load, further wave propagation with damping at the boundaries. Time increments of $\Delta t = 0.002$ s are used (more numerical damping).

4) Static HCA step with a duration of $10^6 \cdot 0.0625$ s = 62,500 s without cyclic loading but with consideration of σ^{static}. The left, right and bottom boundaries of the model are fixed in orthogonal direction for this step.

For the analytical and semi-analytical calculation the half-space is divided into 5 layers with a thickness of 0.2 m from 0 to 1 m below the foundation and 9 layers with a thickness of 1.0 m from 1 to 10 m below the foundation. In a depth ≥ 10 m the strain amplitude ε^{ampl} is so small that no accumulation of permanent strains is expected and no further layers are required. Preliminary investigations showed that even for a much lower number of layers (5-10) the results are independent of the number of layers.

Low cyclic amplitudes

Initially, the focus is on foundations being subjected to low cyclic amplitudes, with a ratio of the cyclic amplitude to the self-weight of the foundation in the range of 1–5 %. This is the range of relevant loading conditions for rotating machines used for grinding or milling as well as vibrations caused by cooling systems. Typically, the cyclic loading is characterised by a high frequency (> 10 Hz) and a large number of load cycles (> 10^6). The high loading frequency necessitates the consideration of inertia effects in the calculation. The amplitude

of the cyclic loading is $\sigma^{\mathrm{dyn}} = 4\ \mathrm{kN}/(\pi \cdot r_0^2) = 0.59$ kPa. Initially, the HCA parameters without considering the threshold strain amplitude given in Table 2 are considered.

Figure 10a displays the vertical displacement of the foundation during the application of 10 cycles, of which in the last cycle the strain path is recorded (dark grey phase). It is well visible that only one cycle is required until a steady-state is reached, which is due to the wave propagation in the system. Following the cyclic loading, the resting period (light grey phase) allows for dissipation of all waves and the foundation comes to rest without having accumulated any permanent settlements. The strain amplitude calculated based on the recorded strain path is given in Fig. 10b for a vertical path below the foundation in the symmetry axis, below the characteristic point and at the corner of the foundation (see Fig. 9). In addition, the distribution resulting from the analytical (simplified) approach using Eqs. (13, 14) is displayed. The analytical approach gives a good approximation of the distributions obtained from the FE analysis but tends to slightly overestimate the strain amplitude below the foundation and in greater depths. For the FE simulation, the strain amplitude in the symmetry axis and below the characteristic point first increases and then decreases with increasing depth below foundation. This is because of the higher stresses or strains close to the foundation corner according to analytical solutions for the stress distribution below rigid foundations (see e.g. Boussinesq's solution). With greater depth the strain amplitude tends to a more homogeneous distribution in radial direction as the loading due to the foundation is spread over a larger soil volume.

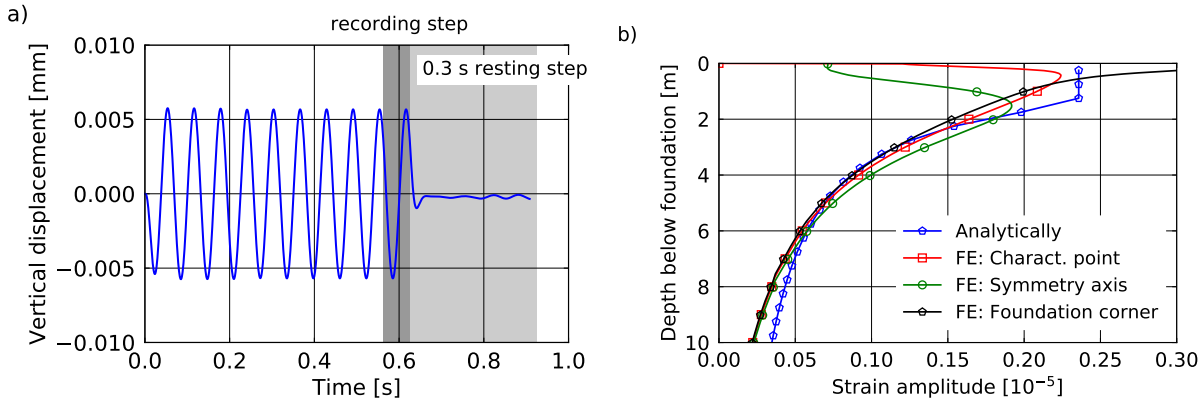

Fig. 10. a) Vertical displacement of the foundation during application of 10 cycles and a subsequent resting phase. The time frame which is used to record the strain path is highlighted in dark grey. b) Vertical path of the strain amplitude $\varepsilon^{\mathrm{ampl}}$ below the foundation given in the symmetry axis, below the characteristic point and at the corner of the foundation for the FE simulation as well as the distribution obtained using the analytical approach.

Following the resting phase, 10^6 cycles are simulated using the HCA model. The settlement of the foundation versus the number of cycles is given in Fig. 11 for the results of the FE simulation, the analytical and the semi-analytical calculation. The strain amplitude below the characteristic point obtained from the FE simulation is used as input in the latter case. A small deviation between the FE simulation and the (semi-)analytical approach is found, which can be attributed to an altered stress ratio due to the self weight

of the foundation not considered in the (semi-)analytical approach. The self-weight of the foundation increases the factor f_Y below the foundation in case of the FE simulation, resulting in higher accumulation rates during the high-cycle phase. This is further discussed in Section *Discussion*.

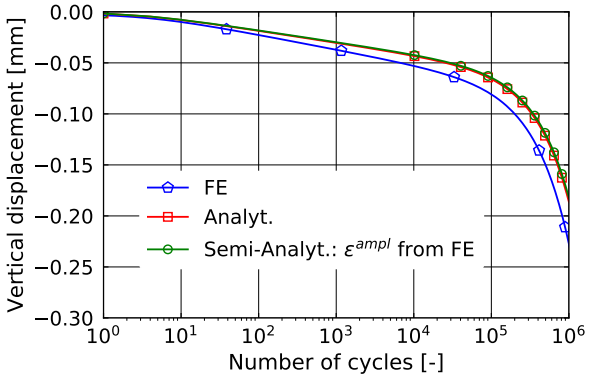

Fig. 11. Vertical displacement of the foundation during the high-cycle phase for the FE simulation and for the analytical approaches using either the strain amplitude distribution obtained by the simplified formula or the distribution calculated in the FE simulation (characteristic point).

For this example the strain amplitudes are in the range of $2 \cdot 10^{-6}$, which is much lower than the threshold strain amplitude levels introduced in Section *Shear strain and threshold shear strain*. Therefore, technically no accumulation of deformations is expected to occur. However, the HCA model nevertheless predicts permanent deformations. This is because the threshold strain amplitude is not considered in the original HCA equations. In the next section the different strategies to incorporate the threshold strain amplitude are analysed.

Large cyclic amplitudes

For some foundations the cyclic loading amplitude is higher than 10 % of its self-weight. In this case, settlement due to the accumulation of permanent strains occurs. An amplitude of $\sigma^{\mathrm{dyn}} = 11.8$ kPa is adopted for the simulations in this section, which is 20-times higher than in the previous section and amounts approximately 25 % of the load due to the total mass of the machine and the foundation. Because the material behaviour is considered fully elastic, the displacements and the strain amplitude are exactly 20-times higher than in the calculations shown in Fig. 10. The results of the analytical calculations and the FE simulation for the high-cycle phase are given in Fig. 12. Compared to the simulations with the lower cyclic amplitude, smaller differences between the analytically calculated settlement and the FE solution exists, and an almost perfect match is found regardless of whether the strain amplitude of the FE simulation is used as input for the analytical calculation or the analytical approach is applied. As will be explained later based on Fig. 17, the accordance is better for the larger cyclic amplitude compared to the lower amplitude because the function f_Y tends to change in the FE simulation towards a value corresponding to a K_0 stress state, which is a priori assumed in the 1D (semi-)analytical analysis. Such

a change in f_Y does not take place for the lower loading amplitude because the stress is almost unaffected by the high-cyclic loading in that case.

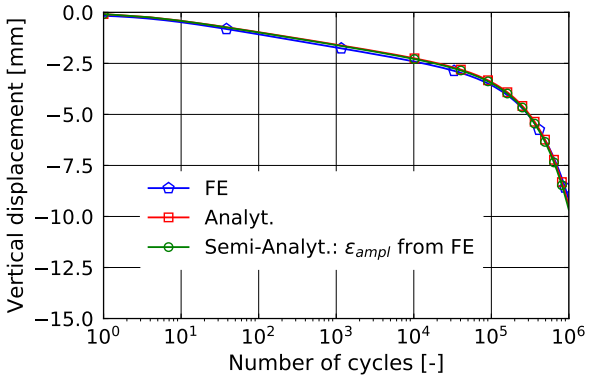

Fig. 12. Vertical displacement of the foundation during the high-cycle phase for $\sigma^{\mathrm{dyn}} = 11.8$ kPa for the FE simulation, the analytical and semi-analytical approach

The different strategies to incorporate the threshold strain amplitude are discussed in the following. In Section *Threshold strain amplitude and its incorporation in the HCA model*, the parameters of the HCA model for Karlsruhe fine sand (KFS) have been (re-)calibrated considering the threshold strain amplitude and are given in Table 2. Figure 13a displays the FE results using the different approaches with the parameters of KFS for $\gamma_{\mathrm{lim}}^{\mathrm{ampl}} = 0$ and $\gamma_{\mathrm{lim}}^{\mathrm{ampl}} = 10^{-5}$, respectively. The parameter set calibrated considering $\gamma_{\mathrm{lim}}^{\mathrm{ampl}} = 10^{-5}$ is denoted as $C_i(\varepsilon_{\mathrm{lim}}^{ampl})$. The other simulations all consider the parameter set derived assuming $\gamma_{\mathrm{lim}}^{\mathrm{ampl}} = 0$. Comparatively large differences between the predicted settlements from the different approaches are observed, despite the relatively low value of $\gamma_{\mathrm{lim}}^{\mathrm{ampl}}$. While the approach with a jump in f_{ampl} (approach No. 1 in Section *Threshold strain amplitude and its incorporation in the HCA model*) gives results very close to the simulations without any consideration of $\gamma_{\mathrm{lim}}^{\mathrm{ampl}}$, the approaches using a smooth function f_{ampl} result in less accumulated deformations. As expected, the approach using the modified parameter set gives slightly larger deformations compared to approach No. 2 using the original parameter set, because the consideration of $\gamma_{\mathrm{lim}}^{\mathrm{ampl}}$ in the calibration necessitates parameters resulting in higher accumulation to fit well to the experimental results.

The difference between the approaches increases with increasing value of $\gamma_{\mathrm{lim}}^{\mathrm{ampl}}$, as is visible from the results of the simulations presented in Figs. 13b and 14a.

Figure 14b compares the semi-analytical results with the FE simulations, using different values of $\gamma_{\mathrm{lim}}^{\mathrm{ampl}}$ in both cases. The strain amplitude obtained from the FE simulation below the characteristic point of the foundation is used for the analytical results and the parameter set for $\gamma_{\mathrm{lim}}^{\mathrm{ampl}} = 0$ is adopted. The differences between the semi-analytical and the FE results are small, proving the suitability of the semi-analytical approach.

The spatial distributions of the function f_{ampl} for the different values of threshold strain amplitude considered in Figs. 13a,b are depicted in Fig. 15. Approach No. 2 is adopted for Figs. 15b,c and the parameter C_{ampl} calibrated considering $\gamma_{\mathrm{lim}}^{\mathrm{ampl}}$ is used for the calculation of f_{ampl}. For $\gamma_{\mathrm{lim}}^{\mathrm{ampl}} = 3 \cdot 10^{-5}$ in Fig. 15c only a very small soil zone below the foundation corner shows values of f_{ampl} larger than zero. Accumulation of permanent deformation

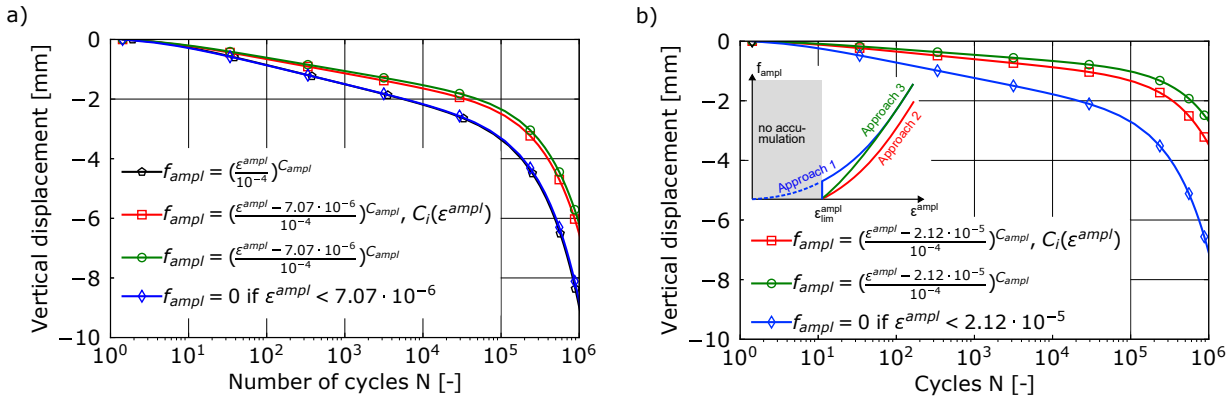

Fig. 13. Vertical displacement of the foundation using different approaches to incorporate the threshold strain amplitude. Plot a) incorporates a threshold shear strain amplitude of $\gamma_{\text{lim}}^{\text{ampl}} = 10^{-5}$ and plot b) a threshold shear strain amplitude of $\gamma_{\text{lim}}^{\text{ampl}} = 3 \cdot 10^{-5}$.

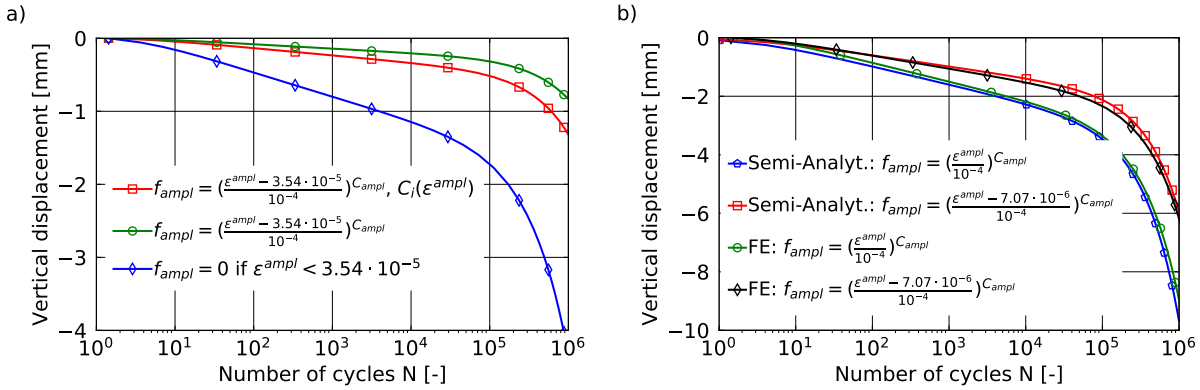

Fig. 14. Plot a): Same as Fig. 13 but using $\gamma_{\text{lim}}^{\text{ampl}} = 5 \cdot 10^{-5}$. Plot b): Comparison of the semi-analytically calculated solution with the FE simulation.

occurs only in this zone, which leads to the lower foundation settlements observed in Fig. 13b for $\gamma_{\text{lim}}^{\text{ampl}} = 3 \cdot 10^{-5}$.

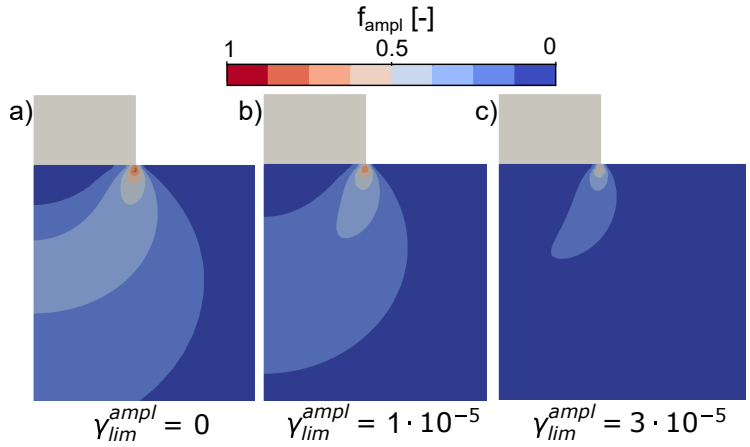

Fig. 15. Spatial distributions of the function f_{ampl} of the HCA model without threshold strain amplitude (plot a) or for different values of the threshold strain amplitude (plots b and c)

Variation of material parameters and loading frequency

In this section, the calculations are performed adopting a HCA parameter set for so-called Berlin sand. This is a well-graded sand with a median grain size of D_{50} of 0.55 mm and a coefficient of uniformity of C_U of 3 which is much more prone to strain accumulation under cyclic loading compared to the KFS. The HCA parameters are given in Table 4.

C_{ampl}	C_e	C_p	C_Y	C_{N1} $[10^{-3}]$	C_{N2}	C_{N3} $[10^{-5}]$
1.7	0.371	0.417	2.573	3.08	0.0166	7.88

Table 4. Parameters of the HCA model for Berlin sand

The results of the analytical calculations and the FE simulation using the same loading as in Section *Large cyclic amplitudes* are given in Fig. 16. Compared to the simulations for KFS, larger differences between the analytically calculated settlement and the FE solution exists, despite using the strain amplitude of the FE simulation as an input for the analytical calculation. The reason for this is the considerably larger settlement, causing the average stress below the foundation to change more with the number of cycles, which is only accounted for by the FE simulation. This stress change influences the functions f_Y and f_p of the HCA model, with the first being the more decisive influencing factor for the deviation of the two solutions. For the first $\approx 1,000$ cycles the solutions are in good agreement because the functions f_Y and f_p still have a similar magnitude in both approaches. It should be noted that a permanent settlement of ≈ 100 mm at $N = 10^6$ would certainly exceed the serviceability of the foundation and the example is for academic purposes, illustrating the limits of the analytical approach.

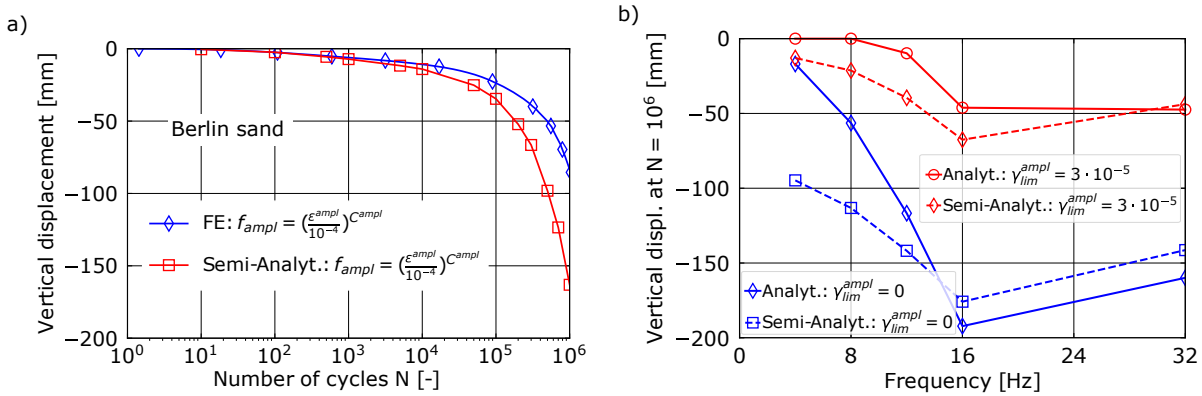

Fig. 16. a) Vertical displacement of the foundation during the high-cycle phase for the FE simulation and the semi-analytical approach adopting the HCA parameters of Berlin sand. b) Vertical displacement of the foundation at $N = 10^6$ for different frequencies of the cyclic load using the analytical and semi-analytical approaches without or with a threshold shear strain amplitude of $\gamma_{\text{lim}}^{\text{ampl}} = 3 \cdot 10^{-5}$.

Up to now, only simulations with a loading frequency of 16 Hz have been discussed. However, as outlined in Section *Analytical approach*, the formulas used to calculate the cyclic velocity amplitude V_z and the shear strain in Eq. (14) are not applicable for arbitrary

frequencies. For instance, if the cyclic loading is very slow, V_z tends to zero, indicating that the shear strain is also negligible. However, in reality, the strain amplitude can still be large, resulting in permanent settlement. Figure 16 shows the vertical displacement of the foundation at $N = 10^6$ for different frequencies of the cyclic load using the analytical and semi-analytical approach without or with a threshold shear strain amplitude of $\gamma_{\text{lim}}^{\text{ampl}} = 3 \cdot 10^{-5}$. The HCA parameters for Berlin sand are adopted. It is well visible that for frequencies $\lessapprox 10$ Hz the full analytical approach results in an underestimation of settlements, which is caused by an underprediction of the values for the shear strain amplitude. The reason that the settlement reduces for larger frequencies is due to a smaller displacement amplitude of the foundation, which is an outcome of Eq. (21). To resolve this issue, the strain amplitude in the analytical approach should be calculated by employing analytical solutions for the stress distribution below a foundation for frequencies $\lessapprox 10$ Hz. The additional stress due to the cyclic loading is then divided by the soil stiffness, giving the strain amplitude. An iterative procedure may be required if the dependence of the stiffness on the strain amplitude is considered.

Discussion

The simulations presented in the previous section demonstrate the suitability of the proposed analytical approach. The calculation of the strain amplitude using the simplified Eq. (13) and Eq. (14) can serve as a basis for a first estimation of the long-term settlement. For more precise predictions and lower load frequencies, however, FE simulations to determine the spatial distribution of the strain amplitude should be performed. These simulations are rather straightforward since they usually can be performed using a linear elastic material. No implementation of the HCA model in a FE software is required for the analytical or semi-analytical approach.

A key difference between the (semi-)analytical and the FE approach is that the factors f_Y and f_p considering the influence of the stress on the accumulation rate change only in the FE simulation. Figure 17 shows the factors f_e, f_Y and f_p at the start of the high-cycle phase ($N = 0$, Fig. 17a) and at $N = 10^6$ (Fig. 17b) using the original parameters of KFS and $\gamma_{\text{lim}}^{\text{ampl}} = 10^{-5}$. The weighting of the three functions in the calculation of the strain accumulation is identical. Therefore, taking into account the range of values, the factor f_Y is the most crucial factor, which varies strongly both spatially and temporarily. Both f_e and f_p vary by 10 % - 20 % spatially and with N while f_Y varies by 500 %. Interestingly, f_Y tends to a more homogeneous distribution with increasing N, which is closer to the distribution assumed in the (semi-)analytical calculation. This explains why the accordance between FE simulation and (semi-)analytical calculation is better for the large loading amplitude considered in Section *Large cyclic amplitudes* compared to the low loading amplitude chosen in Section *Low cyclic amplitudes*. In case of the low loading amplitude, the factor f_Y used in the FE simulation maintains its initial distribution shown in Fig. 17a during the HCA phase, which results in higher accumulation compared to the (semi-)analytical approach.

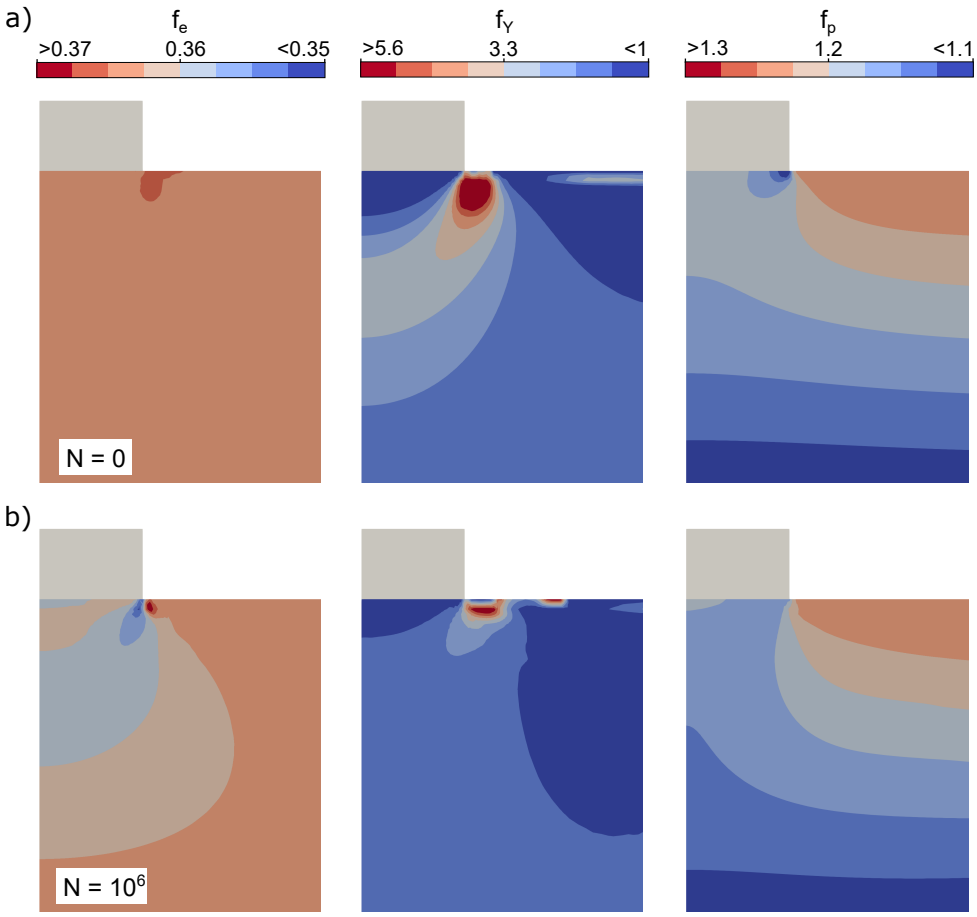

Fig. 17. Spatial distribution of the factors f_e, f_Y and f_p of the HCA model at $N = 0$ (a) and $N = 10^6$ (b) for KFS and $\gamma_{\text{lim}}^{\text{ampl}} = 10^{-5}$

In general, the simplified approaches are only valid if the change in stress due to cyclic loading is small, which means that the settlements of the foundation are also not too large (few centimetres maximum). For most foundations this will be the case, so it is not a relevant shortcoming of the approaches.

From the results presented in Section *Large cyclic amplitudes*, it is clear that the magnitude of the threshold strain amplitude $\gamma_{\text{lim}}^{\text{ampl}}$ and the approach adopted to incorporate it in the HCA model play a key role in predicting the permanent settlements. In general, the approaches Nos. 2 and 3, without a jump in the function f_{ampl}, are considered more meaningful. Approach No. 3 is superior to approach No. 2 because the threshold strain amplitude is accounted for in the calibration process, but it requires a new calibration, which is a disadvantage considering the large database of existing parameter sets for the HCA model (Wichtmann et al., 2015b; Wichtmann, 2016). Therefore, for low values of threshold strain amplitude it is believed that approach No. 2 is sufficient, because the results presented in Section *Large cyclic amplitudes* showed only small differences between approaches Nos. 2 and 3. However, approach No. 3 should be adopted for higher values of threshold strain amplitude. In any case, more experiments with strain amplitudes in the range of the threshold strain and a larger number of loading cycles at these strain levels are required to identify the most suitable approach.

Finally, with respect to application of the proposed schemes to inhomogeneous soil conditions, it is noted that the procedures described in Section *Analytical approach* also hold if soil properties change with depth (changing soil state variables, e.g. density and stress, are captured automatically by the HCA model). The division of the soil in layers should be done in accordance with the natural layering of the soil in this case and the strain amplitude should be calculated with the stiffness (shear wave velocity) of each layer. However, to get a more realistic distribution of strain amplitude, application of the semi-analytical approach is recommended in case of inhomogeneous soils. In this case, no assumption about the depth-distribution of the soil stiffness for calculation of the amplitude of the foundation according to Section *Cyclic displacement and velocity amplitude of the foundation* is required and effects from reflection and refraction can be taken into account. Moreover, constitutive models of arbitrary complexity can be adopted in the semi-analytical approach. Once the strain amplitude is obtained, steps 5-8 as described in Section *Analytical approach* can be performed adopting HCA parameters determined for the different soils, e.g. by means of correlations (Wichtmann et al., 2015b).

Conclusion

Approaches with different complexity to calculate the settlement of foundations subjected to long-term dynamic cyclic loading have been developed and presented in this work. They are based on the HCA model, which is experimentally well validated and its parameters can be obtained by correlation with standard soil parameters (Wichtmann et al., 2015b). The approach can also analogously be used to analyse the long-term response of foundations on cohesive soils, using the HCA model for clay (Wichtmann, 2016; Staubach et al., 2022b; Staubach et al., 2023b). The importance of incorporating a threshold strain amplitude in the HCA model has been demonstrated. Different approaches for this incorporation have been proposed, and the need for future experimental campaigns has been outlined. As a highlight of the presented approach, it can be noted that the analytical approach does not require numerical simulations to perform the settlement analysis.

Data availability statement

All data, models, or code that support the findings of this study are available from the corresponding author upon reasonable request.

List of symbols

a	long side of the foundation
a_0	dimensionless frequency
b	short side of the foundation
C_{ampl}	parameter of the HCA model in function f_{ampl}
C_e	parameter of the HCA model in function f_e
C_p	parameter of the HCA model in function f_p
C_U	Uniformity coefficient
C_Y	parameter of the HCA model in function f_Y
C_{N1}	parameter of the HCA model in function f_N
C_{N2}	parameter of the HCA model in function f_N
C_{N3}	parameter of the HCA model in function f_N
C_1, C_2	Lysmer/Kuhlemeyer damper parameters
$C_{z,\Omega}$	frequency-dependent damper
c_s	shear wave velocity
c_p	compression wave velocity
D	damping ratio
D_{50}	median grain size
$d_{zz,0\to\Omega}$	damper coefficient
E	fourth order stiffness tensor
e^{av}	average void ratio
e_{ref}	reference void ratio
f	loading frequency
f_0	natural frequency
f_{ampl}	function of the HCA model considering the strain amplitude
f_e	function of the HCA model considering the void ratio
f_p	function of the HCA model considering the mean average stress p^{av}
f_Y	function of the HCA model considering the stress ratio
$\dot{f}_N$	function of the HCA model considering the cyclic history
$\dot{f}_N^A$	N-dependent function of the HCA model considering the cyclic history

$\dot{f}_N^B$	constant function of the HCA model considering the cyclic history
f_π	function of the HCA model considering polarization changes
G	scalar shear modulus
h	height of the foundation
g^A	cyclic history state variable of the HCA model
$K_{z,0}$	frequency-independent spring stiffness
$K_{z,\Omega}$	frequency-dependent spring stiffness
$k_{zz,0\to\Omega}$	spring stiffness coefficient
K	lateral stress coefficient
m_F	mass of the foundation
m_M	total mass of the machine
n	factor to consider geometrical damping
$\mathbf{m}$	direction of accumulation
N	number of load cycles
P_0	cyclic vertical load amplitude
p^{av}	average mean effective stress
q^{av}	average deviatoric stress
r_0	radius of the substitute circular foundation
t	physical time
V_z	cyclic velocity amplitude
X	dimension
Y	dimension
$\bar{Y}^{\mathrm{av}}$	normalized average stress ratio
z	depth below foundation

α	Rayleigh coefficient for material damping
β	Rayleigh coefficient for material damping
γ	shear strain
γ_c	shear strain in cyclic triaxial tests
γ_F	specific weight of the foundation
γ_{tl}	linear threshold shear strain
γ_{tv}	volumetric threshold shear strain
$\gamma_{\mathrm{lim}}^{\mathrm{ampl}}$	threshold shear strain amplitude
γ_{xy}	shear strain component
ΔN	increment of N-cycles
Δt	time increment
ε_x	normal strain component
ε_{xy}	shear strain component
ε_y	normal strain component
$\varepsilon^{\mathrm{ampl}}$	strain amplitude
$\varepsilon_{\mathrm{lim}}^{\mathrm{ampl}}$	threshold strain amplitude
$\varepsilon^{\mathrm{acc}}$	scalar accumulated strain
$\varepsilon_v^{\mathrm{acc}}$	volumetric accumulated strain
$\dot{\varepsilon}$	scalar strain rate
$\dot{\boldsymbol{\varepsilon}}^{\mathrm{acc}}$	strain accumulation rate
$\dot{\varepsilon}^{\mathrm{acc}}$	scalar strain accumulation rate
$\dot{\boldsymbol{\varepsilon}}$	strain rate
$\dot{\boldsymbol{\varepsilon}}^{\mathrm{pl}}$	plastic strain rate
η^{av}	average stress ratio
λ	wavelength
ν	Poisson's ratio
ρ	density
$\boldsymbol{\sigma}$	effective stress
σ^{dyn}	stress due to dynamic loading of the foundation
σ_h	horizontal stress component
σ^{static}	stress due to self-weight of the machine and foundation
σ_v	vertical stress component

$\dot{\boldsymbol{\sigma}}$ effective stress rate

Ω excitation angular frequency

References

Achenbach, J. D. (1980). *Wave propagation in elastic soils*. Amsterdam: North-Holland, Publ. Comp.

Birrell, M., C. Pastén, J. A. Abell, and R. Astroza (2022). "Probabilistic characterization of a high-cycle accumulation model for sands". In: *Computers and Geotechnics* 147, p. 104798. ISSN: 0266-352X.

Byrne, P. and J. McIntyre (1994). "Deformation in granular soils due to cyclic loading". In: *Geotechnical Special Publication No. 40*. Texas A&M University.

DGGT, ed. (2018). *Empfehlungen des Arbeitskreises 1.4 "Baugrunddynamik" der Deutschen Gesellschaft für Geotechnik e.V.*

Dobry, R. and T. Abdoun (2015). "3rd Ishihara Lecture: An investigation into why liquefaction charts work: A necessary step toward integrating the states of art and practice". In: *Soil Dynamics and Earthquake Engineering* 68, pp. 40–56.

François, S., C. Karg, W. Haegeman, and G. Degrande (2010). "A numerical model for foundation settlements due to deformation accumulation in granular soils under repeated small amplitude dynamic loading". In: *International Journal for Numerical and Analytical Methods in Geomechanics* 34.3, pp. 273–296.

Gazetas, G. (Sept. 1991). "Formulas and Charts for Impedances of Surface and Embedded Foundations". In: *Journal of Geotechnical Engineering* 117.9, pp. 1363–1381.

Haupt, W. (1986). *Bodendynamik*. Braunschweig / Wiesbaden: Vieweg und Sohn.

Hsu, C.-C. and M. Vucetic (2004). "Volumetric threshold shear strain for cyclic settlement". In: *Journal of Geotechnical and Geoenvironmental Engineering, ASCE* 132.1, pp. 58–70.

Jamiolkowski, M., R. Lancellotta, D. C. F. Lo Presti, and O. Pallara (1994). "Stiffness of Toyoura Sand at Small and Intermediate Strain". In: *13th ICSMFE, New Dehli*. Vol. 1, pp. 169–172.

Lentz, R. W. and G. Y. Baladi (1981). "Constitutive Equation for Permanent Strain of Sand Subjected to Cyclic Loading". In: *Transportation Research Record*. Vol. 810, pp. 50–54.

Li, D. and E. T. Selig (1996). "Cumulative Plastic Deformation for Fine-Grained Subgrade Soils". In: *Journal of Geotechnical Engineering* 122.12, pp. 1006–1013. ISSN: 0733-9410.

Machaček, J., P. Staubach, M. Tafili, H. Zachert, and T. Wichtmann (2021). "Investigation of three sophisticated constitutive soil models: From numerical formulations to element tests and the analysis of vibratory pile driving tests". In: *Computers and Geotechnics* 138, p. 104276. ISSN: 18737633.

Machaček, J. (2020). *Contributions to the Numerical Modelling of Saturated and Unsaturated Soils*. Dissertation, Publications of the Institute of Soil Mechanics and Rock Mechanics, Karlsruhe Institute of Technology, Issue No. 187.

Narsilio, G. A. and J. C. Santamarina (2008). "Terminal densities". In: *Geotechnique* 58.8, pp. 669–674. ISSN: 00168505.

Niemunis, A., T. Wichtmann, and T. Triantafyllidis (2005). "A high-cycle accumulation model for sand". In: *Computers and Geotechnics* 32.4, pp. 245–263.

Pais, A. and E. Kausel (1988). "Approximate formulas for dynamic stiffnesses of rigid foundations". In: *Soil Dynamics and Earthquake Engineering* 7.4, pp. 213–227. ISSN: 0267-7261.

Pasten, C., H. Shin, and J. C. Santamarina (2014). "Long-term foundation response to repetitive loading". In: *Journal of Geotechnical and Geoenvironmental Engineering, ASCE* 140.4.

Richart, F., J. Hall, and R. D. Woods (1970). *Vibrations of Soils and Foundations*. Englewood Cliffs, New Jersey: Prentice-Hall.

Sawicki, A. and W. Świdziński (1989). "Mechanics of a sandy subsoil subjected to cyclic loadings". In: *Int. J. Numer. Anal. Meth. Geomech.* 13, pp. 511–529.

Schmüdderich, C., J. Machaček, L. F. Prada-Sarmiento, P. Staubach, and T. Wichtmann (2022). "Strain-dependent slope stability for earthquake loading". In: *Computers and Geotechnics* 152, p. 105048. ISSN: 0266-352X.

Staubach, P., J. Machaček, L. Tschirschky, and T. Wichtmann (Feb. 2022a). "Enhancement of a high-cycle accumulation model by an adaptive strain amplitude and its application to monopile foundations". In: *International Journal for Numerical and Analytical Methods in Geomechanics* 46.2, pp. 315–338. ISSN: 0363-9061.

Staubach, P., I. Kimmig, J. Machaček, T. Wichtmann, and T. Triantafyllidis (2023a). "Deep vibratory compaction simulated using a high-cycle accumulation model". In: *Soil Dynamics and Earthquake Engineering* 166, p. 107763. ISSN: 0267-7261.

Staubach, P., J. Machaček, M. Tafili, and T. Wichtmann (Mar. 2022b). "A high-cycle accumulation model for clay and its application to monopile foundations". In: *Acta Geotechnica* 17.3, pp. 677–698. ISSN: 1861-1125.

Staubach, P., J. Machaček, and T. Wichtmann (June 2022c). "Mortar contact discretisation methods incorporating interface models based on Hypoplasticity and Sanisand: Application to vibratory pile driving". In: *Computers and Geotechnics* 146, p. 104677. ISSN: 0266352X.

Staubach, P., L. Tschirschky, J. Machaček, and T. Wichtmann (2023b). "Monopile installation in clay and subsequent response to millions of lateral load cycles". In: *Computers and Geotechnics* 155, p. 105221. ISSN: 0266-352X.

Vucetic, M. (1994). "Cyclic threshold shear strains in soils". In: *Journal of Geotechnical Engineering, ASCE* 120.12, pp. 2208–2228.

Vucetic, M. and R. Dobry (1988). "Degradation of marine clays under cyclic loading". In: *Journal of Geotechnical Engineering, ASCE* 114.2, pp. 133–149.

Wegener, D. (2013). "Ermittlung bleibender Bodenverformungen infolge dynamischer Belastung mittels numerischer Verfahren". PhD thesis. Institut für Geotechnik, Technische Universität Dresden, Issue No. 17.

Wegener, D. and I. Herle (2012). "Ermittlung von Scherdehnungen durch Schwingungsmessungen und numerische Berechnungen". In: *BAW-Mitteilungen No. 95*. ISSN 21909199, pp. 59–69.

Wichtmann, T. (2005). *Explicit accumulation model for non-cohesive soils under cyclic loading*. PhD thesis, Publications of the Institute of Foundation Engineering and Soil Mechanics, Ruhr-University Bochum, Issue No. 38.

Wichtmann, T. (2016). *Soil Behaviour Under Cyclic Loading: Experimental Observations, Constitutive Description and Applications*. Habilitation, Institute of Soil Mechanics and Rock Mechanics, Karlsruhe Institute of Technology, Issue No. 181.

Wichtmann, T., M. A. Navarrete Hernández, and T. Triantafyllidis (2015a). "On the influence of a non-cohesive fines content on small strain stiffness, modulus degradation and damping of quartz sand". In: *Soil Dynamics and Earthquake Engineering* 69, pp. 103–114. ISSN: 0267-7261.

Wichtmann, T., A. Niemunis, and T. Triantafyllidis (2005). "Strain accumulation in sand due to cyclic loading: drained triaxial tests". In: *Soil Dynamics and Earthquake Engineering* 25.12, pp. 967–979.

Wichtmann, T., A. Niemunis, and T. Triantafyllidis (2009). "Validation and calibration of a high-cycle accumulation model based on cyclic triaxial tests on eight sands". In: *Soils and Foundations* 49.5, pp. 711–728.

Wichtmann, T., A. Niemunis, and T. Triantafyllidis (2010). "On the determination of a set of material constants for a high-cycle accumulation model for non-cohesive soils". In: *Int. J. Numer. Anal. Meth. Geomech.* 34.4, pp. 409–440.

Wichtmann, T. and T. Triantafyllidis (2013). "Effect of uniformity coefficient on G/Gmax and damping ratio of uniform to well graded quartz sands". In: *Journal of Geotechnical and Geoenvironmental Engineering, ASCE* 139.1, pp. 59–72.

Wichtmann, T., A. Niemunis, and T. Triantafyllidis (2015b). "Improved simplified calibration procedure for a high-cycle accumulation model". In: *Soil Dynamics and Earthquake Engineering* 70.3, pp. 118–132. ISSN: 02677261.